Blob- and hole-like structures outstanding during the transition from attached to detached divertor states in GAMMA 10/PDX

H. Tanaka, M. Sakamoto, N. Ezumi, K. Nojiri, A. Terakado, T. Mikami, Y. Kinoshita, K. Kobayashi, M. Yoshikawa, J. Kohagura, and N. Ohno

Citation: Physics of Plasmas **25**, 082505 (2018); doi: 10.1063/1.5040800

View online: https://doi.org/10.1063/1.5040800

View Table of Contents: http://aip.scitation.org/toc/php/25/8

Published by the American Institute of Physics

Blob- and hole-like structures outstanding during the transition from attached to detached divertor states in GAMMA 10/PDX

H. Tanaka,[1,a)] M. Sakamoto,[2] N. Ezumi,[2] K. Nojiri,[2] A. Terakado,[2] T. Mikami,[2] Y. Kinoshita,[2] K. Kobayashi,[2] M. Yoshikawa,[2] J. Kohagura,[2] and N. Ohno[1]
[1]*Graduate School of Engineering, Nagoya University, Chikusa-ku, Nagoya 464-8603, Japan*
[2]*Plasma Research Center, University of Tsukuba, 1-1-1 Tennodai, Tsukuba 305-8577, Japan*

(Received 21 May 2018; accepted 18 July 2018; published online 3 August 2018)

We have measured multipoint fluctuations inside a divertor simulation experimental module (D-module) during the transient discharge from attached to detached states in the tandem mirror device GAMMA 10/PDX. It was first observed that blob-/hole- like positive/negative spikes of the ion saturation current appeared non-periodically around the radially outer side edge on the V-shaped target plate. This tendency became outstanding in the transient state, and the typical speed and size of the isolated blob-like structures in the azimuthal direction were estimated. Additionally, lower-frequency periodic mode fluctuations and their changes due to plasma detachment were investigated not only in the D-module but also in the central cell with the microwave interferometer, etc. Odd and even modes continuously appeared during the discharge, in the range of several kilohertz. *Published by AIP Publishing*. https://doi.org/10.1063/1.5040800

I. INTRODUCTION

Plasma detachment is a promising solution for achieving sufficient reduction of the divertor heat flux in future fusion reactors, e.g., DEMO. Under the detached divertor condition, electron temperature (T_e) and particle flux decrease mainly due to the radiation and recombination processes.[1] Since ion particle flux could be attributed to a non-negligible heat load due to the surface recombination, particularly in low-T_e plasmas, an accurate prediction of the particle flux in the detached plasma is one of the important issues, along with the plasma heat load reduction.

In several magnetic confinement devices, including the tokamak, helical, and linear devices, there are many reports on cross-field transport with filaments, so-called "blobby plasma transport," in the edge region.[2] Such cross-field transport in the radial direction broadens the particle flux across the magnetic field and reduces the peak value on the divertor plate. Furthermore, the enhancement of the cross-field transport is reported around the detached divertor plasmas.[3–9] In addition, recent edge plasma simulation with the SOLPS code suggests that an enhanced cross-field transport coefficient inside the divertor region is necessary for reproducing the footprint profile in the detached divertor experiment.[10] This enhanced cross-field transport leads to the further reduction in the particle-flux peak. To date, the enhancing mechanism and its onset condition are unclear. In order to advance our understanding of physics, comparison of transport behaviors between different magnetic configurations should be valid.

In this study, we have carried out multipoint fluctuation measurements in the tandem mirror device GAMMA 10/PDX. In the tandem mirror configuration, there has been no observation of blobby plasma transport yet. In order to capture the successive change of fluctuation characteristics with respect to the detachment progress, the divertor plasma condition was altered from the attached to detached states during a long-pulse discharge with massive gas puffing. Rollover of the particle flux was observed, and we first confirmed blob-/hole- like positive/negative events inside the "divertor simulation experimental module (D-module)" and its outstanding behavior during the rollover. We applied several statistical analysis techniques and compared the results with those obtained in other magnetic confinement devices. In addition, mode behaviors inside the core and edge regions with the change of the divertor condition were investigated.

In Sec. II, the experimental setup with the measurement system will be introduced. In Sec. III, statistical analysis results will be described. Finally, we will discuss the results obtained in Sec. IV and summarize them in Sec. V.

II. EXPERIMENTAL SETUP

GAMMA 10/PDX is a 27-m length tandem mirror device that equips the D-module on the divergent magnetic field geometry in the west end cell.[11] In this study, a transition from attached to detached states was achieved by a massive H_2 puffing with the plenum pressure of 800 mbar in a 400 ms long-pulse plasma discharge (shot number: 243740). In the past studies, 800 mbar was known to be sufficient for the heat and particle flux reductions due to the plasma detachment.[12–14] The discharge gas species was H_2. Plasma was sustained by the ion cyclotron range of frequency waves, with the total deposited power of ~335 kW.

During the discharge, edge fluctuations were mainly investigated with the Langmuir probes inside the D-module, as shown in Fig. 1. There were 13 electrodes embedded on the upper-side V-shaped target made of tungsten (W). In Fig. 1(b), the axial position (z) is defined to take a zero value at the corner of the V-shaped target. Two probes (#17 and #18) were located upstream of probe #5 almost along the magnetic field with slight deviation in the azimuthal direction, in

[a)]E-mail: h-tanaka@ees.nagoya-u.ac.jp

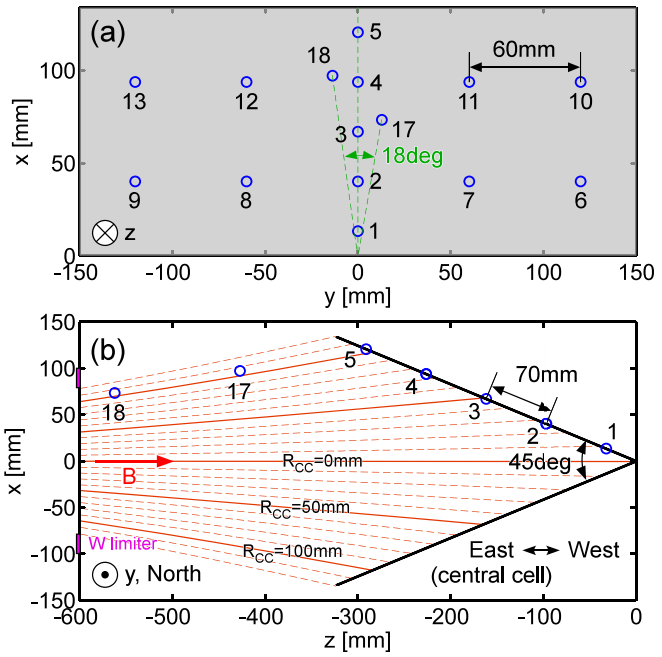

FIG. 1. Positions of Langmuir probes in the D-module viewed from (a) the central cell and (b) the north side.

order to avoid the shadow effect from the upstream probes. Radii in the central cell (R_{CC}) of the magnetic field lines connecting to probes #5, 17, and 18 were $R_{CC} = 106$ mm. Each Langmuir probe had a cylindrical shape, with a diameter of 1.5 mm and a length of 1.1 mm. By applying negative biases, ion saturation current (I_{sat}) fluctuations were acquired with the sampling frequency of 500 kHz. Because I_{sat} is proportional to the electron density and the square root of the electron temperature, I_{sat} fluctuation is strongly affected by the electron density fluctuation. The W limiter was located at the entrance of the D-module. The W limiter, the V-shaped target, and the housing of the D-module were grounded to the vacuum vessel electrically.

In the central cell, electron density fluctuation at the radial center ($R_{CC} = 0$) was obtained with the gold neutral beam probe (GNBP).[15] In addition, the electron line density (NL_{CC}) and the floating potential (V_f) fluctuations were measured with the microwave interferometer (MI) on the midplane ($x = 0$) and the Langmuir probe fixed at the limiter radius ($R_{CC} = 180$ mm), respectively. MI also measured line densities at the west anchor (NL_{WA}) and west barrier cells (NL_{WB}), which were located between the central cell and the west end cell. The magnetic field pointed to the west side from the central cell in this study.

III. FLUCTUATION ANALYSIS

Figures 2(a) and 2(b) show the time series of diamagnetism in the central cell (DM_{CC}), NL_{CC}, NL_{WA}, and NL_{WB}. Plasma was generated from $t \sim 50$ ms. After $t \sim 170$ ms, NL_{WB} increased; then, DM_{CC} decreased by 10–20% and NL_{WA} increased with a finite time delay, which was attributed to the slow penetration of H_2 gas injected from near the D-module. Figure 2(c) shows the spectrogram of NL_{CC}. Before $t \sim 200$ ms, a spectral peak at $f \sim 4$–5 kHz was

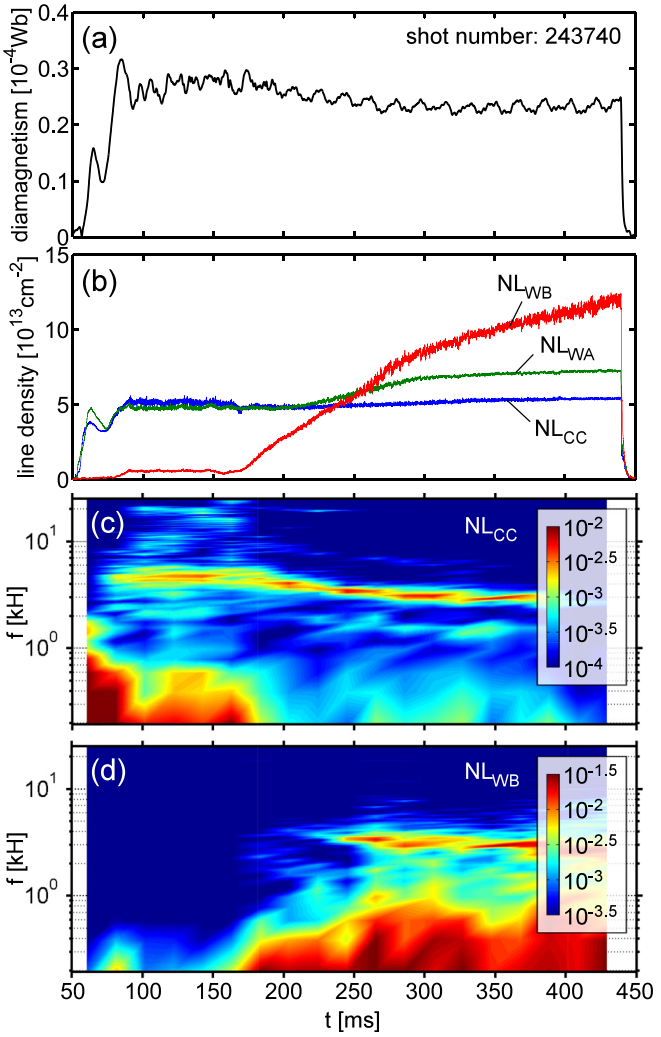

FIG. 2. Time series of (a) DM_{CC}, (b) NL_{CC} (blue), NL_{WA} (green), and NL_{WB} (red). Spectrograms of (c) NL_{CC} and (d) NL_{WB}.

observed. After that, the spectral-peak frequency began to decrease and reached $f \sim 3$ kHz at $t \sim 300$ ms, although the NL_{CC} amplitude was not changed much [see Fig. 2(b)]. Therefore, there was some instability from the beginning of the discharge, and its frequency was influenced due to the gas puffing. The spectrogram of NL_{WB} had the same spectral peak after $t \sim 200$ ms, as shown in Fig. 2(d), indicating that the fluctuation propagation and/or detection around the edge region became easier because of the density increase. On the other hand, we cannot observe such periodic fluctuation from the GNBP signal at $R_{CC} = 0$ (no figure).

Figure 3 shows a time series of I_{sat} signals at probes #3, 4, 5, and 17. In the same figure, simple moving averages ($\langle I_{sat} \rangle$) with a time window of 10 ms are also drawn by the dashed lines. We can see that all $\langle I_{sat} \rangle$ increased from $t \sim 145$ ms. Subsequently, $\langle I_{sat} \rangle$ on the V-shaped target saturated and then decreased [see Figs. 3(a)–3(c)], in contrast with the increase at the upstream probe [see Fig. 3(d)]. This rollover on the V-shaped target resulted from the plasma detachment. Hereinafter, for convenience, we will refer to the periods before and after the rollover as "attached" and "detached" states, respectively. Additionally, the I_{sat}-saturating period

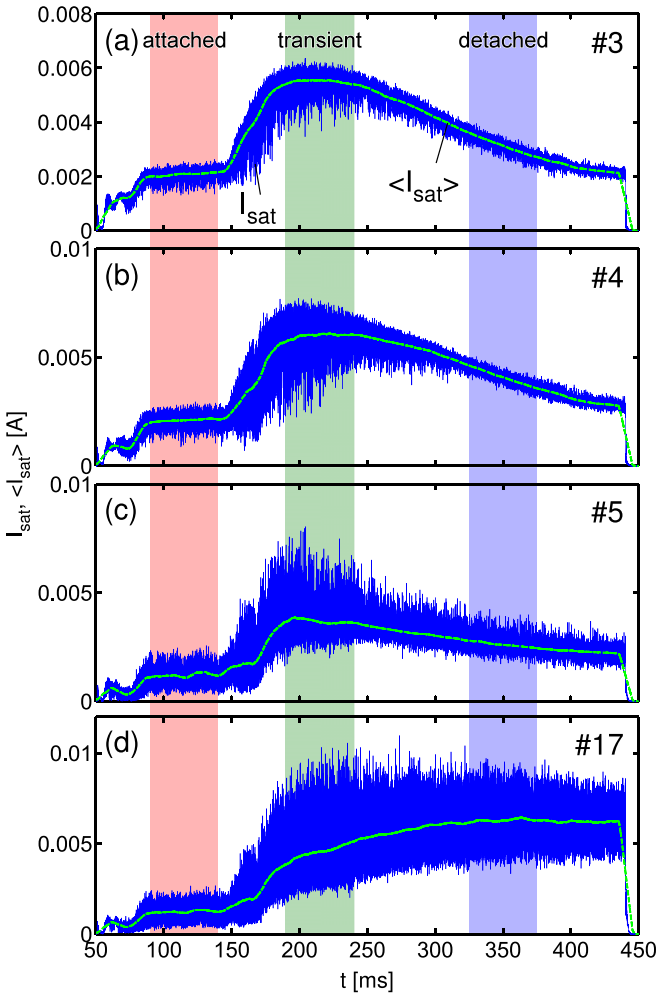

FIG. 3. Time series of raw (solid line) and moving averaged I_{sat} (dashed line) at probe (a) #3, (b) #4, (c) #5, and (d) #17.

during the rollover on the V-shaped target will be called the "transient" state in this study. In the transient state, large negative and positive spikes from $\langle I_{sat}\rangle$ were seen at probes #4 and 5, respectively.

Figure 4(a) shows the $\langle I_{sat}\rangle$ profile along z at probes #1–5, 17, and 18 in the attached ($t\sim115$ ms), transient ($\sim$215 ms), and detached states ($\sim$350 ms). In the attached state, $\langle I_{sat}\rangle$ at probe #5, which was radially and axially far from the high-performance plasma in the central cell, was smallest. In the transition phase, the $\langle I_{sat}\rangle$ profile was not changed much, but its amplitude became 2–4 times larger. In the detached state, $\langle I_{sat}\rangle$ at upstream probes #17 and 18 continued to increase, while $\langle I_{sat}\rangle$ on the V-shaped target decreased.

Figure 4(b) shows the skewness defined by $S\equiv\langle I_{sat}^3\rangle/\langle I_{sat}^2\rangle^{3/2}$. In all states, positive and negative S can be found at the upstream and downstream from probes #4–5, respectively. Positive/negative S indicates that positive/negative spikes are dominant in a fluctuation. Such spikes of I_{sat} are interpreted as blobs with higher density and holes with lower density. In JET tokamak, blobs and holes are generated just inside the separatrix where strong poloidal flow shear exists.[16] Although there was no separatrix between probes #4 and #5 in GAMMA 10/PDX, these probes were located just inside the W limiter [see Fig. 1(b)], and flow

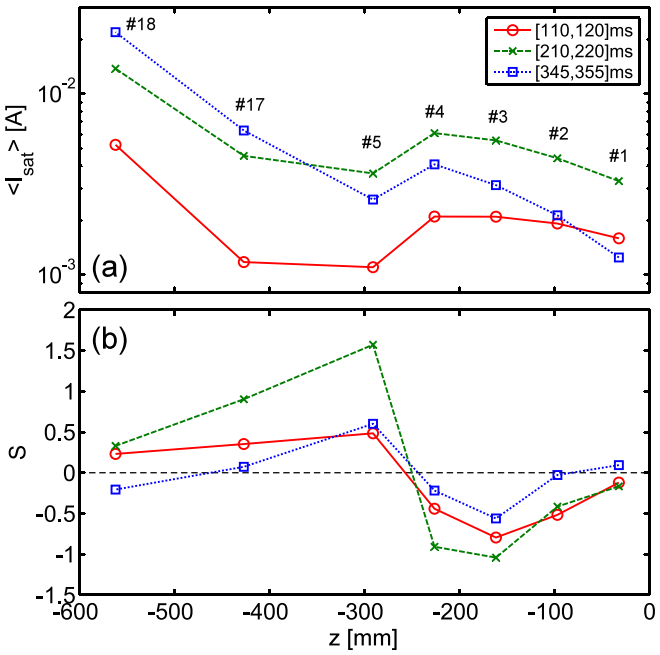

FIG. 4. (a) $\langle I_{sat}\rangle$ and (b) S at attached (solid line), transient (dashed line), and detached states (dotted line) as a function of z.

shear might exist. It should be noted that $|S|$ amplitudes became high in the transient state compared with those in the attached and detached states. Therefore, blob- and hole-like structures generated on the magnetic field lines near the W limiter could be enhanced in the transient state.

In order to determine the frequency characteristics, we applied the Fourier transform, as shown in Fig. 5. We can find a spectral peak at $f\sim2.2$ kHz in the attached state, although NL_{CC} had a clear peak at 4–5 kHz in Fig. 2(c). The $\sim$2.2 kHz fluctuation was also confirmed with the segmented limiter plates in the central cell with somewhat weak amplitude, and its azimuthal mode number (m) seemed to be $m=1$, rotating in the counter-clockwise direction viewed from the central cell in Fig. 1(a). In the higher-frequency region, we can see the shoulders consisting of flat and inclined shapes, e.g., at $f\sim30$ kHz in probes #5, 17, and 18. Such a shoulder, which is often observed in the blob study,[17] appears when the spikes with a characteristic duration time appear non-periodically in a fluctuation.[18] At probes #3–4, the frequencies of the shoulders were lower.

In the transient state, the spectral peak at several kilohertz disappeared, which seems to be buried in the enhanced high-frequency fluctuation with the shoulder. It should be noted that a small convex is observed at $f\sim30$ kHz at probe #17. After the rollover, in contrast, clear peaks at 1.5, 3, and 4.5 kHz appeared in the detached states. The 1.5 kHz fluctuation was also confirmed in V_f with large amplitude at the limiter radius in the central cell (no figure). At probes #17 and 18, shoulders were observed at $f\sim60$ kHz. This might be affected by the fluctuation in the central cell because $\langle I_{sat}\rangle$ increased and S became $\sim$0 in the detached state (see Fig. 4). A small convex at $f\sim40$–120 kHz and a sharp peak at $f=100$ kHz were also confirmed at probes with a small number (e.g., #1–3), where I_{sat} signals were weak. The amplitudes of the convex and the sharp peak were small before

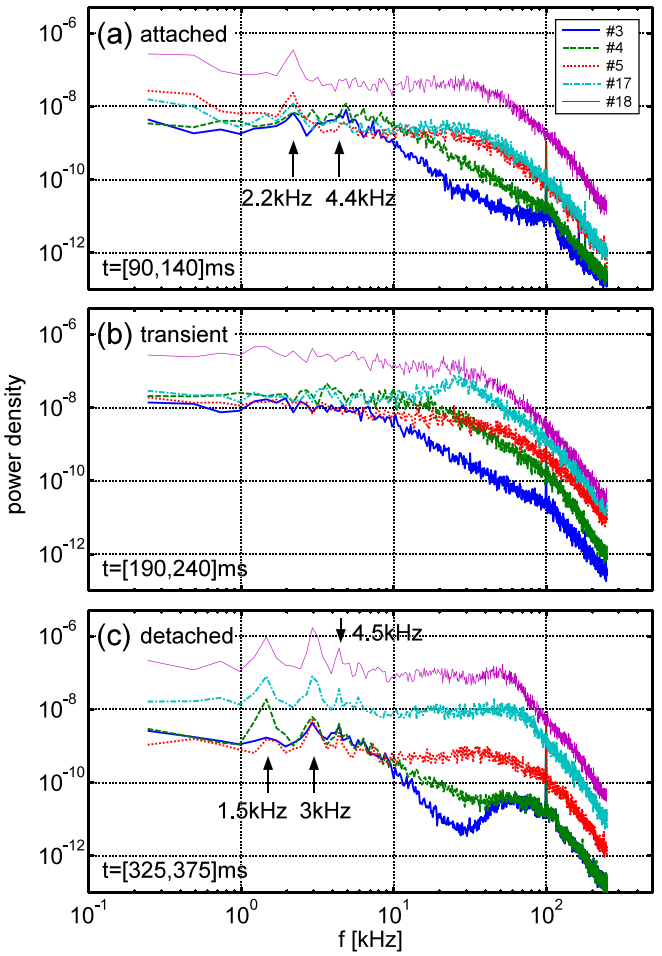

FIG. 5. Power spectra of I_{sat} at probes #3 (solid line), 4 (dashed line), 5 (dotted line), 17 (dashed dotted line), and 18 (thin line) in (a) attached, (b) transient, and (c) detached states.

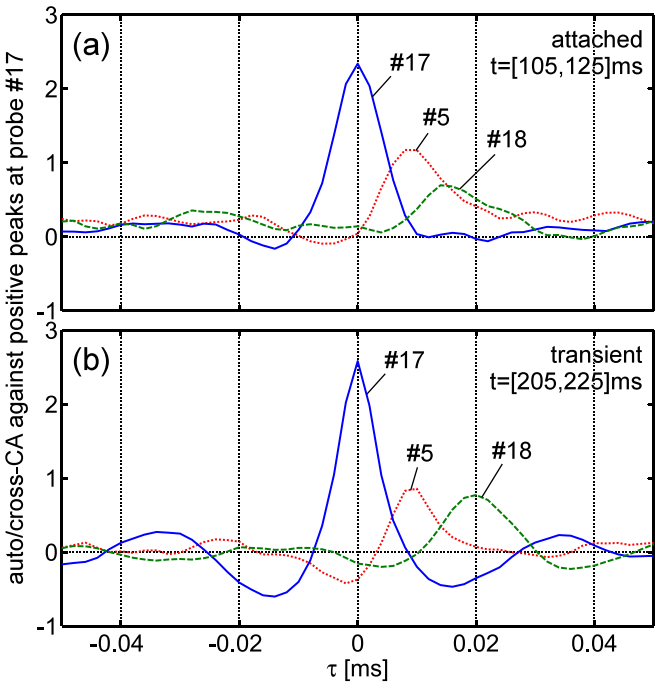

FIG. 6. Normalized auto-CA shape at probes #17 (solid line) and cross-CA shapes at probe #5 (dotted line) and 18 (dashed line) in (a) attached and (b) transient states.

and after the discharge and became large during the discharge; this was possibly due to some noises from the discharge operation.

In order to investigate the spikes composed of the high-frequency components, the conditional averaging (CA) technique was employed. Before using the CA method, moving normalization[19] was applied with the time window of 10 ms by subtracting the moving average and dividing by the moving standard deviation. Figure 6 shows the auto-CA shape of probe #17 and cross-CA shapes of probes #5 and 18. Here, positive spikes were detected when peaks of the moving normalized I_{sat} at probe #17 exceeded +2. After that, subsets of self/other normalized fluctuation around the detected time points were extracted and averaged in the same time domain as τ. In the attached and transient states, 90 and 202 time points were detected, respectively. It is found that auto-CA shape at probe #17 appears without the periodic behavior in the attached state. On the other hand, in the transient state, quasi-periodicity is seen, corresponding to the existence of the spectral convex in Fig. 5(b). The duration between local minimums sandwiching the central peak was 26–30 μs, which is comparable with the well-observed time scale of blobs in tokamaks.[16,17,20]

Cross-CA shapes at probes #5 and 18 have positive spikes appearing in series after the positive spike at probe #17. A similar temporal relation was also confirmed by using the correlation analysis (no figure). Considering the positional relationship of probes #17, 5, and 18 in Fig. 1(a), positive spikes rotated in the counter-clockwise direction viewed from the central cell. The time delays between probes #17 and 18 were estimated as 14 and 20 μs in the attached and transient states, respectively. By assuming that the parallel propagation speed of the fluctuation was much faster than the rotation speed, rotation frequencies (rotation speeds at probe #17) can be calculated as 3.6 kHz (2.2 km/s) and 2.5 kHz (1.5 km/s) in the attached and transient states, respectively. The estimated rotation frequencies are similar values to those of the periodic fluctuations in Fig. 5. By using the rotation frequency and the duration time, the azimuthal mode number and azimuthal length could be estimated as $m > 10$ and 45–60 mm at probe #17 position, respectively.

Auto-CA was also calculated to extract the typical-spike shapes at probes #3–5, where negative and positive S are clearly found in Fig. 4(b), in the transient state. Here, 79 and 77 negative spikes were averaged with the threshold of –2 for the normalized fluctuations at probes #3 and 4, respectively. At probe #5, 172 time points were detected with the threshold value of +2. From Fig. 7, it is noted that a several-times longer duration time was observed at a probe with a smaller number, corresponding to the lower frequency of the shoulder in Fig. 5(b). Such a large difference in the duration time between positive and negative spikes is not observed in the tokamak device.[16] The longer duration time of the typical hole-like structure might be attributed to a slower rotation speed near the radial center with the same rotation frequency, which contributes to the longer staying time of a finite-size structure at a fixed position.

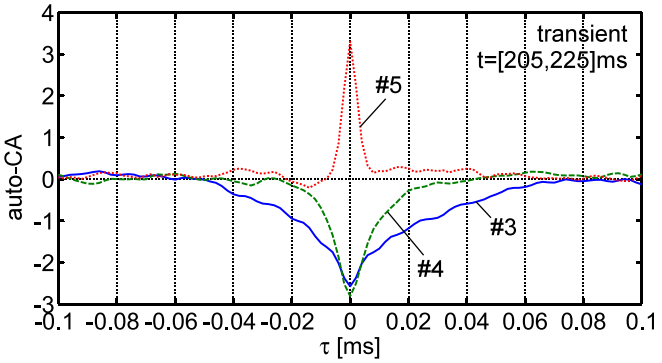

FIG. 7. Normalized auto-CA shapes at probes #3 (solid line), 4 (dashed line), and 5 (dotted line) in the transient state.

IV. DISCUSSION

We have estimated the azimuthal velocity of blob-like structures. However, we cannot assess the radial motion because there was no significant correlation between radially distant neighboring probes (#3–5). The typical size of the blob-like structures in the radial direction would be small compared with the probe interval. In addition, the radial speed might not be so high compared with the azimuthal speed. The CA results clarified that the blob-/hole- like structures were mostly isolated with a single peak. The estimated rotation frequency of the blob-like structures was comparable with the frequencies of periodic fluctuations caused by the mode rotation. Therefore, isolated blob-like structures and mode structures might move on the same flow in the azimuthal direction.

The typical duration time of the blob-like positive spikes in the transient state was not so different from the attached one, as shown in Fig. 6. On the other hand, in the linear plasma device NAGDIS-II, frequency characteristics between both states are substantially different.[9] Considering that the duration time would reflect the azimuthal speed largely in GAMMA 10/PDX, the change of the radial electric field (E_r) from attached to transient states might be smaller if the azimuthal speed was determined by the $E_r \times B$ drift near the birth place of blob-like structures. We should try to measure the E_r near the D-module and discuss it, considering the rotation speed in future.

In the transient state compared to the attached one, fluctuation amplitudes and $|S|$ became larger, whereas the duration time was not so different. In ASDEX-U tokamak, enhancement of the blobby plasma transport in the scrape-off layer (SOL) was reported when the divertor collisionality was high.[21,22] In the high divertor collisionality case including the high recycling and divertor detachment cases, the sheath limited regime transitions to the inertial filamentary regime, and consequently the polarization inside blobs, which drives the radial transport, becomes strong. In this study, polarization inside the blob-like structures could be generated due to the centrifugal force and/or the neutral wind effect,[23] in a similar manner to other linear devices. Furthermore, the polarization might be enhanced due to the high divertor collisionality. In relation to the generation of the blob-like structures, a little convex observed at probe #17 in Fig. 5(b) would be a hint to clarify the generation mechanism.

In the several kilohertz range, Langmuir probes and MI had periodic fluctuations at different frequencies; for example, the $f \sim 2.2$ kHz peak in the attached state and $f \sim 1.5$ kHz peak in the detached state measured with the Langmuir probes were not clearly seen in the MI signal. Because the MI signal was line-integrated at the midplane, fluctuations with odd modes became invisible due to the offsetting; in contrast, even modes should be emphasized. Considering the frequency ratio of spectral peaks and the above-described analysis result from the segmented limiter plates, it is natural that the azimuthal mode numbers of 2.2/1.5 kHz and 4.4/3 kHz in the attached/detached state are $m = 1$ and 2, respectively.

V. SUMMARY

We have investigated the relationship between the cross-field transport and the plasma detachment in the tandem mirror device GAMMA 10/PDX. Blob- and hole-like structures accompanying positive and negative spikes of I_{sat}, respectively, were first confirmed at radially outer-side probes inside the D-module. These fluctuations became significant with larger skewness during the rollover in the transient state, and there were similarities and differences with results in other magnetic confinement devices.

We are planning to analyze two-dimensional fast camera data to extract the spatial profiles of the detected fluctuations viewed from the north side from the D-module. In addition, it is necessary to evaluate the internal electric field inside the blob-/hole- like structure and the double-vortex potential structure[24] for a detailed comparison with the blobby plasma transport. Furthermore, this study suggests that higher-spatial resolution is required for detecting the radial motion of blob-/hole- like structures.

ACKNOWLEDGMENTS

This work was supported by JSPS KAKENHI (16H06139 and 16H02440), the NIFS Collaboration Research program (NIFS16KUGM108 and NIFS17KUGM120), and the NINS program of Promoting Research by Networking among Institutions (01411702).

[1]N. Ohno, Plasma Phys. Controlled Fusion **59**, 034007 (2017).
[2]D. A. D'Ippolito, J. R. Myra, and S. J. Zweben, Phys. Plasmas **18**, 060501 (2011).
[3]B. Stansfield, F. Meo, G. Abel, C. Boucher, J.-L. Gauvreau, J. P. Gunn, E. Haddad, J.-L. Lachambre, J. Mailloux, R. Marchand *et al.*, J. Nucl. Mater. **241–243**, 739 (1997).
[4]S. Potzel, M. Wischmeire, M. Bernert, R. Dux, H. W. Müller, A. Scarabosio, and ASDEX Upgrade Team, J. Nucl. Mater. **438**, S285 (2013).
[5]H. Tanaka, N. Ohno, Y. Tsuji, S. Kajita, S. Masuzaki, M. Morisaki, H. Tsuchiya, A. Komori, and LHD Experimental Group, Phys. Plasmas **17**, 102509 (2010).
[6]E. M. Hollmann, D. G. Whyte, D. Nishijima, N. Ohno, Y. Uesugi, and N. Ezumi, Phys. Plasmas **8**, 3314 (2001).
[7]N. Ohno, K. Furuta, and S. Takamura, J. Plasma Fusion Res. **80**, 275 (2004).
[8]T. Onda, S. Kajita, T. Iijima, A. Tonegawa, N. Ohno, and H. Tanaka, Contrib. Plasma Phys. **57**, 87 (2017).
[9]H. Tanaka, K. Takeyama, M. Yoshikawa, S. Kajita, N. Ohno, and Y. Hayashi, Plasma Phys. Controlled Fusion **60**, 075013 (2018).

[10]F. Reimold, M. Wischmeire, M. Bernert, S. Potzel, A. Kallenbach, H. W. Müller, B. Sieglin, U. Stroth, and ASDEX Upgrade Team, J. Nucl. Mater. **463**, 128 (2015).
[11]Y. Nakashima, K. Ichimura, M. S. Islam, M. Sakamoto, N. Ezumi, M. Hirata, M. Ichimura, R. Ikezoe, T. Imai, T. Kariya *et al.*, Nucl. Fusion **57**, 116033 (2017).
[12]M. S. Islam, Y. Nakashima, H. Matsuura, K. Ichimura, M. M. Islam, K. Shimizu, K. Fukui, M. Ohuchi, K. Nojiri, A. Terakado *et al.*, Plasma Fusion Res. **11**, 2402042 (2016).
[13]K. Nojiri, M. Sakamoto, N. Ezumi, S. Togo, A. Terakado, K. Ichimura, M. Yoshikawa, J. Kohagura, and Y. Nakashima, Proc. AIP Conf. **1771**, 060008 (2016).
[14]M. Sakamoto, A. Terakado, K. Nojiri, N. Ezumi, Y. Nakashima, K. Sawada, K. Ichimura, M. Fukumoto, K. Oki, K. Shimizu *et al.*, Nucl. Mater. Energy **12**, 1004 (2017).
[15]M. Mizuguchi, M. Yoshikawa, Y. Miyata, S. Goshu, M. Nakada, Y. Ooho, Y. Nakashima, and T. Imai, Rev. Sci. Instrum. **79**, 10F309 (2008).
[16]G. S. Xu, V. Naulin, W. Fundamenski, C. Hidalgo, J. A. Alonso, C. Silva, B. Goncalves, A. H. Nielsen, J. J. Rasmussen, S. I. Krasheninnikov *et al.*, Nucl. Fusion **49**, 092002 (2009).
[17]G. Y. Antar, G. Counsell, Y. Yu, B. Labombard, and P. Devynck, Phys. Plasmas **10**, 419 (2003).
[18]H. Tanaka, N. Ohno, N. Asakura, Y. Tsuji, H. Kawashima, S. Takamura, Y. Uesugi, and JT-60U Team, Nucl. Fusion **49**, 065017 (2009).
[19]H. Tanaka, N. Ohno, Y. Tsuji, S. Kajita, S. Masuzaki, M. Kobayashi, T. Morisaki, A. Komori, and LHD Experimental Group, Plasma Fusion Res. **7**, 1402152 (2012).
[20]J. A. Boedo, D. Rudakov, R. Moyer, S. Krasheninnikov, D. Whyte, G. McKee, G. Tynan, M. Schaffer, P. Stangeby, P. West *et al.*, Phys. Plasmas **8**, 4826 (2001).
[21]D. Carralero, G. Birkenmeier, H. W. Müller, P. Manz, P. deMarne, S. H. Müller, F. Reimold, U. Stroth, M. Wischmeier, E. Wolfrum, and ASDEX Upgrade Team, Nucl. Fusion **54**, 123005 (2014).
[22]D. Carralero, M. Siccinio, M. Komm, S. A. Artene, F. A. D'Isa, J. Adamek, L. Aho-Mantila, G. Birkenmeier, M. Brix, G. Fuchert *et al.*, Nucl. Fusion **57**, 056044 (2017).
[23]S. I. Krasheninnikov and A. I. Smolyakov, Phys. Plasmas **10**, 3020 (2003).
[24]D. A. D'Ippolito, J. R. Myra, S. I. Krasheninnikov, G. Q. Yu, and A. Y. Pigarov, Contrib. Plasma Phys. **44**, 205 (2004).